

## Supporting information

# Order-disorder transition in nano-rutile TiO<sub>2</sub> anodes: A high capacity low-volume change Li-ion battery material

*Christian Kolle Christensen,<sup>a</sup> Mohammad Aref Hasen Mamakhet,<sup>b</sup> Ananya Renuka Balakrishna,<sup>c</sup> Bo Brummerstedt Iversen,<sup>b</sup> Yet-Ming Chiang,<sup>c</sup> Dorthe Bomholdt Ravnsbæk<sup>a,\*</sup>*

<sup>a</sup> Department of Physics, Chemistry and Pharmacy, University of Southern Denmark, Campusvej 55, 5230 Odense M, Denmark

<sup>b</sup> Center for Materials Crystallography, Department of Chemistry and iNANO, Aarhus University, Langelandsgade 140, 8000 Aarhus C, Denmark

<sup>c</sup> Department of Materials Science and Engineering, Massachusetts Institute of Technology, 77 Massachusetts Ave., Cambridge, MA 02139, USA

**Table S1.** Overview of known ambient-condition TiO<sub>2</sub> polymorphs

Name	Space group	Unit cell (Å)				vol/Z (Å <sup>3</sup> )	Reference
		<i>a</i>	<i>b</i>	<i>c</i>	β (°)		
Anatase	<i>I4<sub>1</sub>/amd</i>	3.79	3.79	9.51	90	34.15	<sup>1-3</sup>
Rutile	<i>P4<sub>2</sub>/mnm</i>	4.59	4.59	2.96	90	31.18	<sup>1-3</sup>
Brookite	<i>Pbca</i>	9.17	5.46	5.14	90	32.17	<sup>1,2,4</sup>
TiO <sub>2</sub> -B (bronze)	<i>C2/m</i>	12.17	3.74	6.51	107.3	35.31	<sup>1,2,5</sup>
TiO <sub>2</sub> -H (hollandite)	<i>I4/m</i>	10.18	10.18	2.97	90	38.47	<sup>1,2,6</sup>
TiO <sub>2</sub> -R (ramsdellite)	<i>Pbnm</i>	4.90	9.46	2.96	90	34.30	<sup>1,7</sup>
TiO <sub>2</sub> -II (columbite)	<i>Pbcn</i>	4.52	5.5	4.94	90	30.70	<sup>1,2,8</sup>
TiO <sub>2</sub> -III (baddeleyite)	<i>P2<sub>1</sub>/c</i>	4.64	4.76	4.81	99.2	26.22	<sup>1,9</sup>

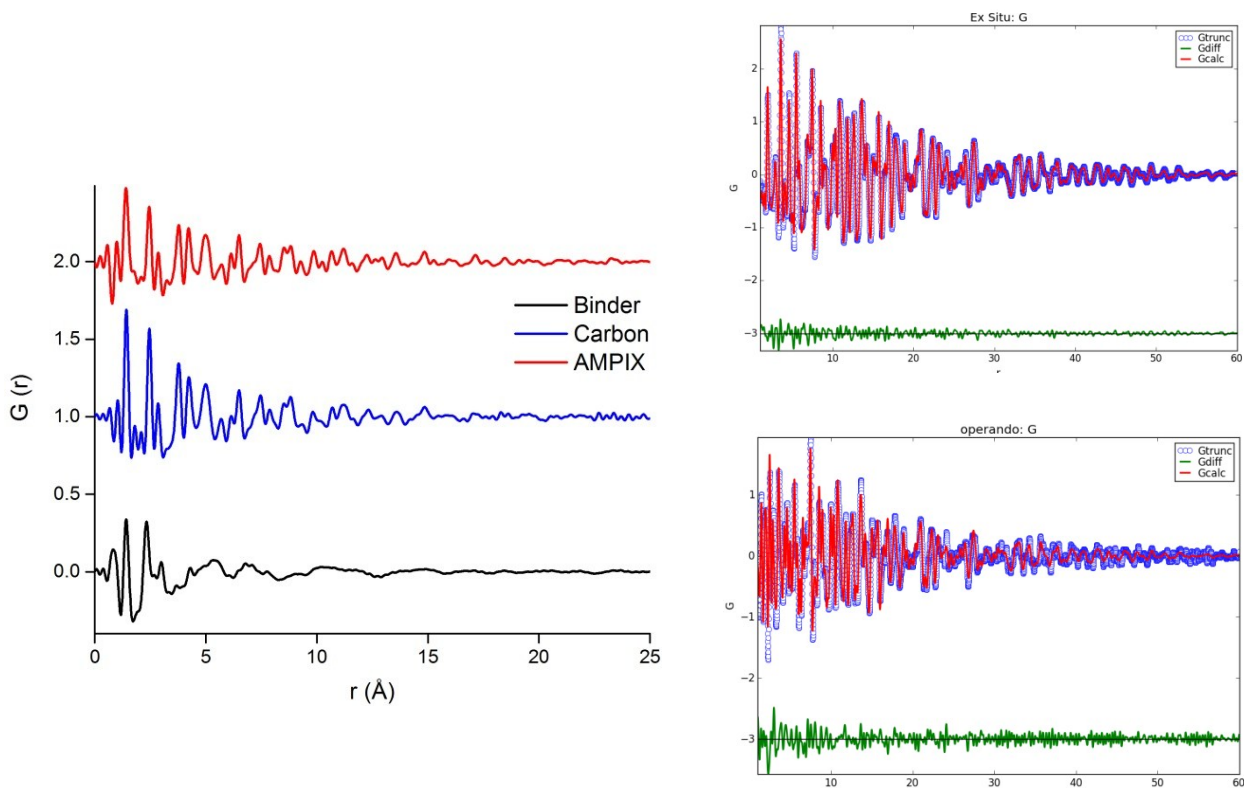


**Figure S1.** (Left) PDFs of electrode additives used in this study: PVDF binder (black), conductive carbon Super C45 (blue) as well as the AMPIX cell only containing the separator and electrolyte (red). The latter configuration serves as background and is used for reciprocal space background subtraction. Above  $\sim 7 \text{ \AA}$  the signals are reduced and comparable to the noise level. Below  $7 \text{ \AA}$  the conductive carbon and the AMPIX cell (i.e. remaining background signal arising from possible non-complete background subtraction) contribute with six peaks; two relatively sharp and intense at  $1.42 \text{ \AA}$  and  $2.45 \text{ \AA}$ , and four less intense and less sharp at  $2.85 \text{ \AA}$ ,  $3.77 \text{ \AA}$ ,  $4.23 \text{ \AA}$  and  $4.99 \text{ \AA}$ . (Right) Comparison of PDF fits of the pristine rutile  $\text{TiO}_2$  structure using data from ex situ measurements of the pure as-synthesized material (top) and from first scan of the operando PDF experiment of an electrode pellet within the AMPIX cell (bottom). The latter fit ( $R_w = 0.29$ ) includes a graphite structure as a second phase and is naturally not as good as for the ex situ data ( $R_w = 0.12$ ), as the signal intensity is decreased, and background noise caused by the AMPIX cell is increased. Consequently, a significantly reduction in the signal to noise ratio appears. In the residual plots the noise display a higher frequency, in  $r$ , for the operando compared with ex situ measurements. This sums up to a larger  $R_w$ , even though the fit is still relatively good.

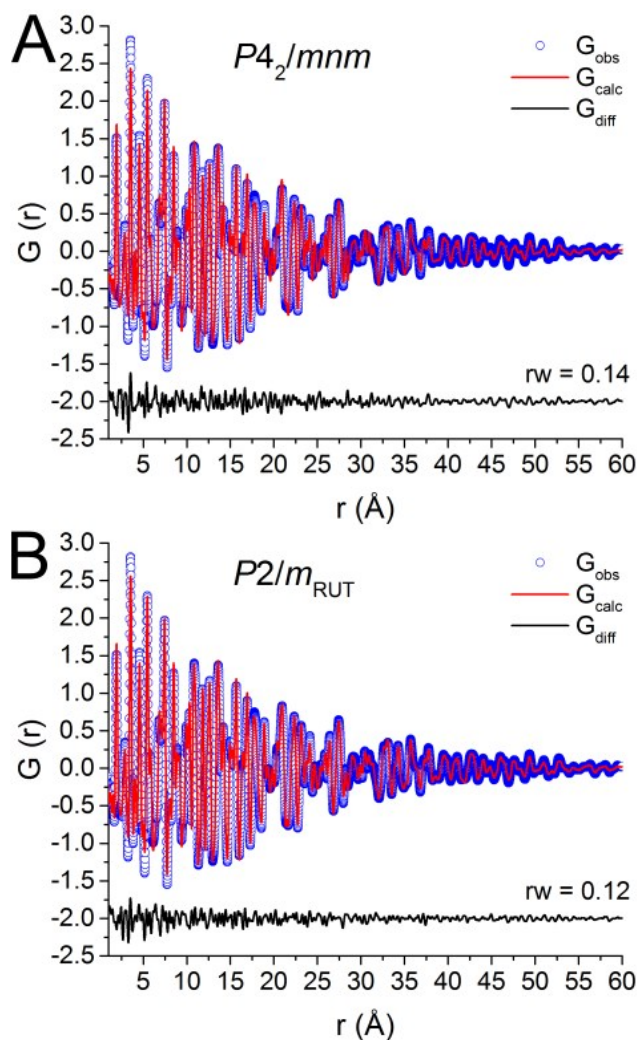


**Figure S2.** Pair distribution function (PDF) analysis obtained from total X-ray scattering (TXS) data of the as prepared rutile  $\text{TiO}_2$ . In (A) the PDF is fitted using an undistorted tetragonal  $P4_2/mnm$  model while in (B) a distorted monoclinic rutile-like  $P2/m_{\text{RUT}}$  structure model is used.

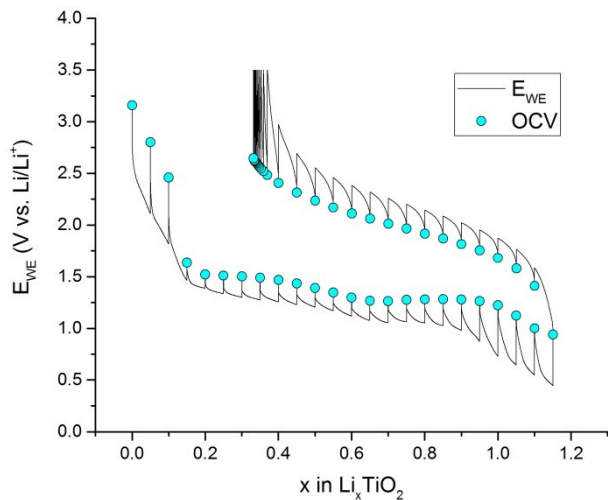
Cell parameters			
$a$ ( $\text{\AA}$ )	4.6061(19)	diameter ( $\text{\AA}$ )	100(14)
$b$ ( $\text{\AA}$ )	4.6061(19)	$\text{Ti U}_{\text{iso}} (\text{\AA}^2)$	0.0052(5)
$c$ ( $\text{\AA}$ )	2.9627(23)	$\text{O U}_{\text{iso}} (\text{\AA}^2)$	0.0117(18)

Atom positions			
	x/a	y/b	z/c
Ti	0	0	0
Ti	$\frac{1}{2}$	$\frac{1}{2}$	$\frac{1}{2}$
O	0.3061(26)	0.3061(26)	0
O	0.6938(26)	0.6938(26)	0
O	0.1938(26)	0.8061(26)	$\frac{1}{2}$
O	0.8061(26)	0.1938(26)	$\frac{1}{2}$

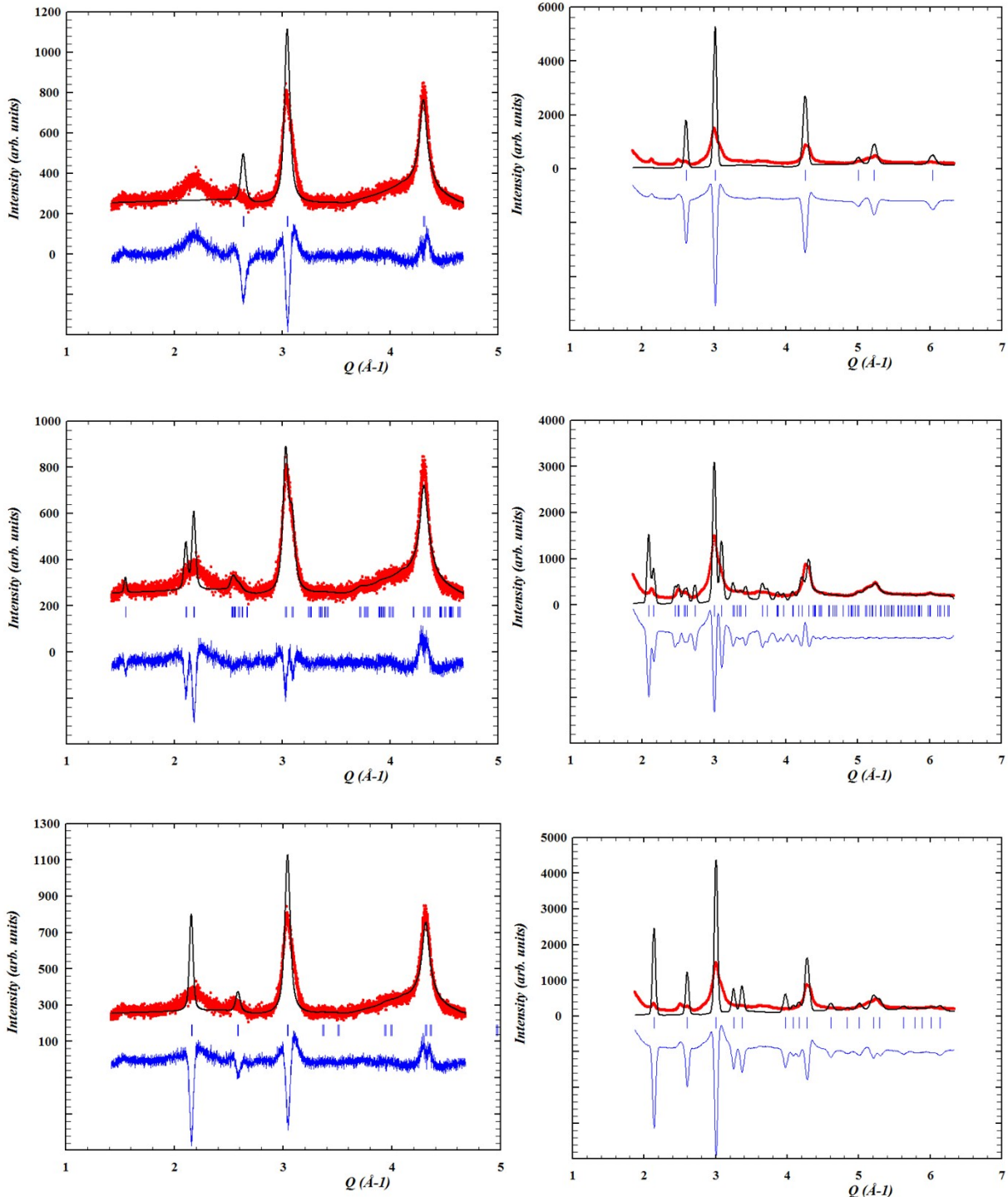
Cell parameters			
$a$ ( $\text{\AA}$ )	4.6251(50)	diameter ( $\text{\AA}$ )	113(20)
$b$ ( $\text{\AA}$ )	2.9623(22)	$\text{Ti U}_{\text{iso}} (\text{\AA}^2)$	0.0047(6)
$c$ ( $\text{\AA}$ )	4.5844(55)	$\text{O U}_{\text{iso}} (\text{\AA}^2)$	0.0102(25)
$\beta$ ( $^\circ$ )	90.24(22)		

Atom positions			
	x/a	y/b	z/c
Ti	0	0	0
Ti	$\frac{1}{2}$	$\frac{1}{2}$	$\frac{1}{2}$
O	0.3064(12)	0	0.3228(13)
O	0.6936(12)	0	0.6772(13)
O	0.1910(12)	$\frac{1}{2}$	0.7852(12)
O	0.8090(12)	$\frac{1}{2}$	0.2148(12)

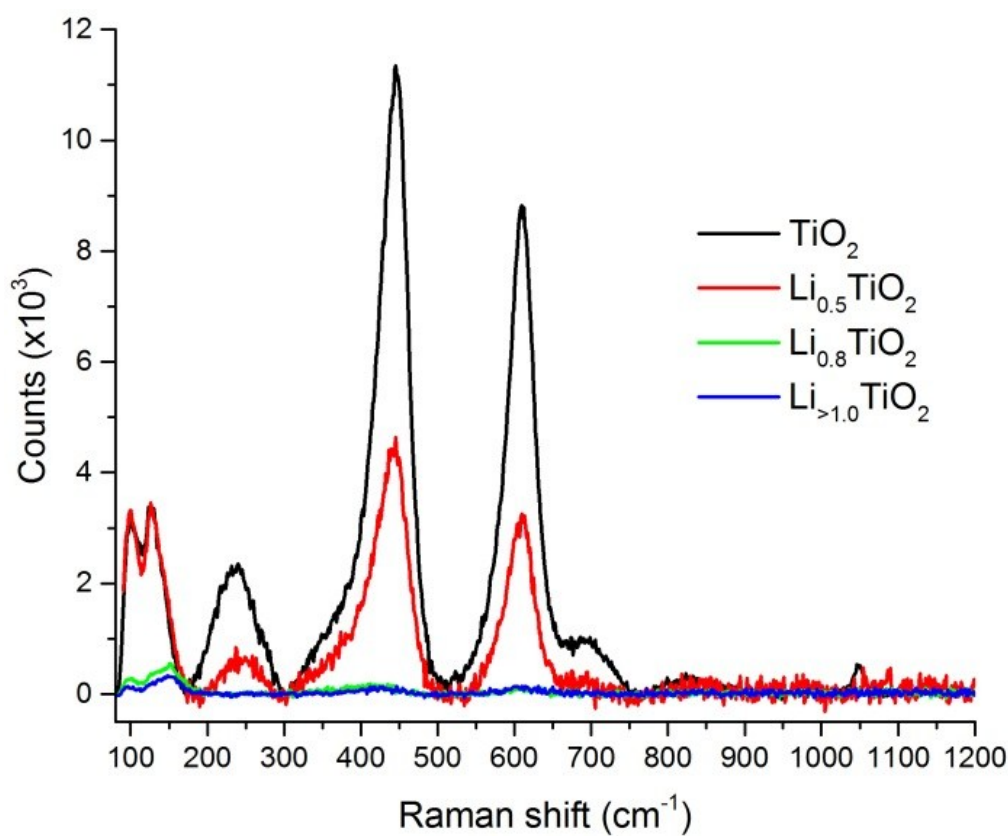
**Table S2.** Result of PDF using (Top) an undistorted tetrahedral  $P4_2/mnm$  model and (bottom) a distorted monoclinic rutile-like  $P2/m_{\text{RUT}}$  structure model.



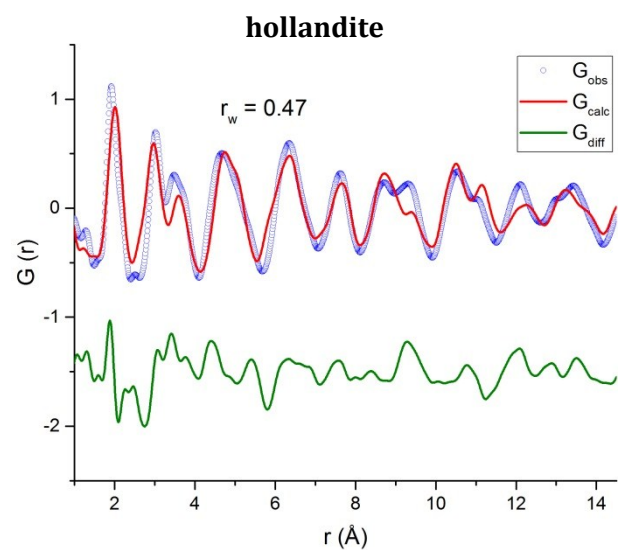
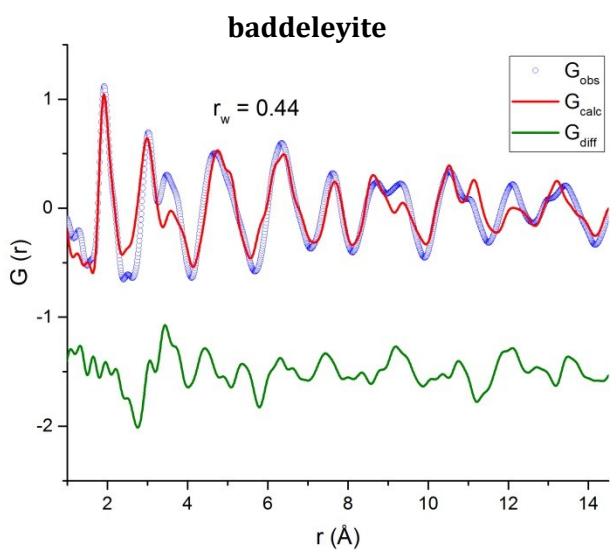
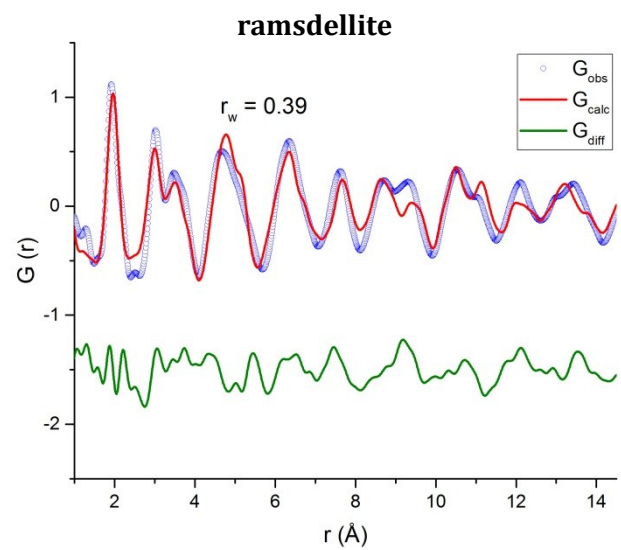
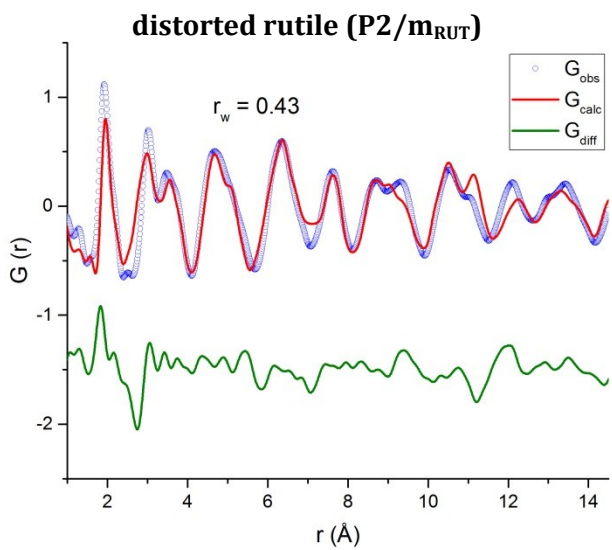
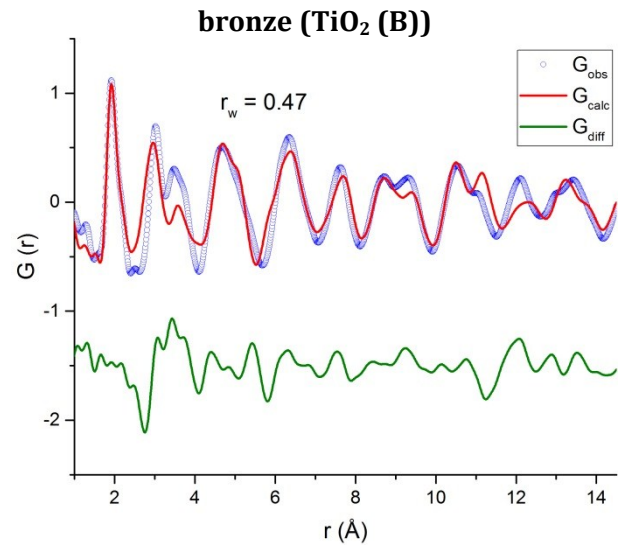
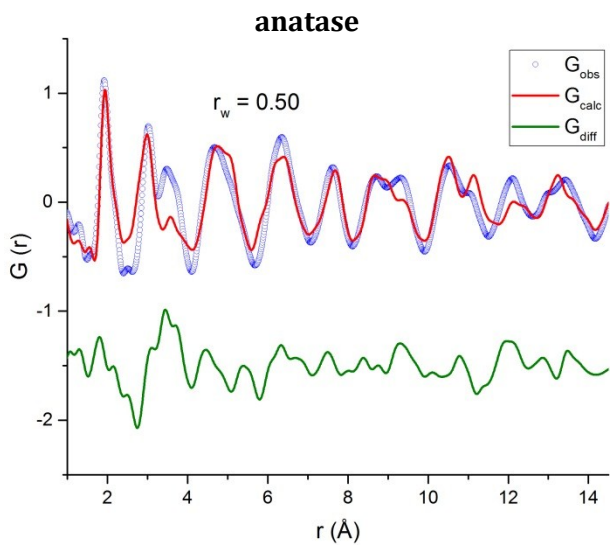
**Figure S3.** Galvanostatic intermittent titration (GITT) of 13 nm rutile  $\text{TiO}_2$  vs. Li, each current step lasts 0.5h @ C/10 rate followed by 4.5 h rest. The GITT curve shows that the over potential at rate C/10 is around 0.25V. A potential plateau at 1.5 V from  $x = 0.2$  to  $0.45$  in  $\text{Li}_x\text{TiO}_2$  is observed in agreement with the Galvanostatic test, and a second plateau at 1.3 V from  $x = 0.65$  to  $0.95$  in  $\text{Li}_x\text{TiO}_2$  is slightly lower Li-content than in the Galvanostatic test. On charge no plateaus are observed.



**Figure S4.** Le Bail fit of (left) *ex situ* PXD data ( $\text{Cu K}\alpha$ ) for the chemically lithiated rutile with composition  $\text{Li}_{-1}\text{TiO}_2$  and (right) *operando* PXD data ( $\lambda = 0.2173 \text{ \AA}$ ) taken at the end of the first discharge, i.e.  $x\text{Li} \sim 0.93$  in  $\text{Li}_x\text{TiO}_2$ . The data is fitted by a (top)  $Fm\text{-}3m$  cell ( $a = 4.1282(4) \text{ \AA}$ ), (middle) a monoclinic  $P2/m$  cell ( $a = 5.0144(19) \text{ \AA}$ ,  $b = 2.88262(5) \text{ \AA}$ ,  $c = 5.0769(11) \text{ \AA}$  and  $\beta = 72.575(14)^\circ$ ) and (bottom) another monoclinic  $P2/m$  cell ( $a = 3.39(3) \text{ \AA}$ ,  $b = 2.4345(17) \text{ \AA}$ ,  $c = 2.938(7) \text{ \AA}$  and  $\beta \sim 142.3(4)^\circ$ ). The cell parameters are from refinement of the *ex situ* data. The peak profiles are kept narrow in order to highlight peak positions.



**Figure S5.** Raman spectra of chemically lithiated 13 nm rutile  $\text{TiO}_2$ , (black) pristine sample, (red, green and blue) 0.5, 1.0 and 1.5 equivalent of *n*-butyllithium added.



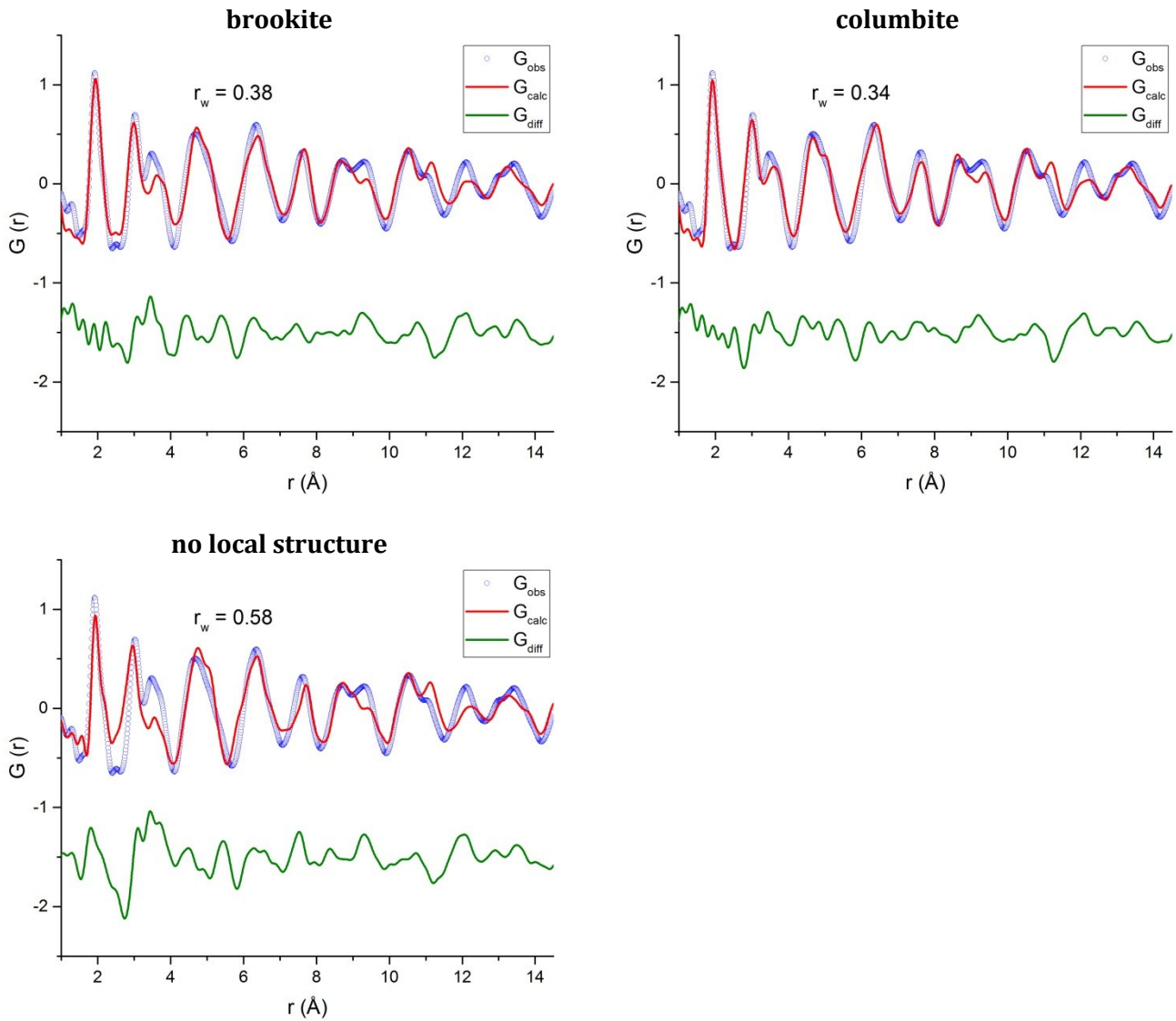


**Figure S6.** Fits of the PDF obtained from total X-ray scattering of the chemical lithiated rutile with composition  $\text{Li}_{-1}\text{TiO}_2$ . All fits include a layered  $\alpha\text{-NaFeO}_2$ -like  $\text{LiTiO}_2$  phase with particle size of  $\sim 50$  Å, while small domains of  $\sim 5$  nm of different  $\text{TiO}_2$  polymorph are included in the fits: From the top the fits include: Anatase, Bronce ( $\text{TiO}_2(\text{B})$ ), distorted rutile ( $P2/m_{\text{RUT}}$ ), ramsdellite, baddeleyite, hollandite, brookite, and columbite. For comparison, the bottom fit includes only the  $\alpha\text{-NaFeO}_2$ -like  $\text{LiTiO}_2$  phase, i.e. no local structure.

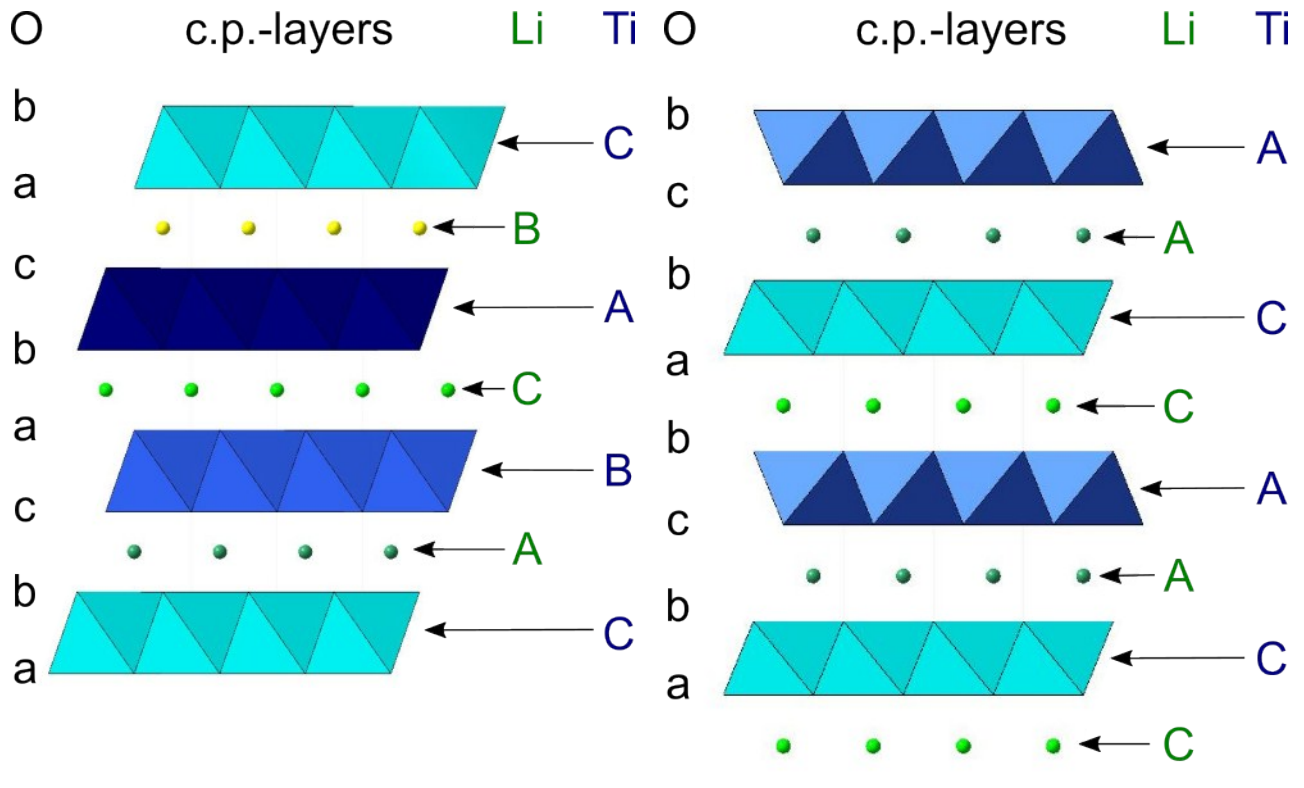


**Figure S7.** close packed stacking sequence of O3-type and O2-type AMO<sub>2</sub> structures.

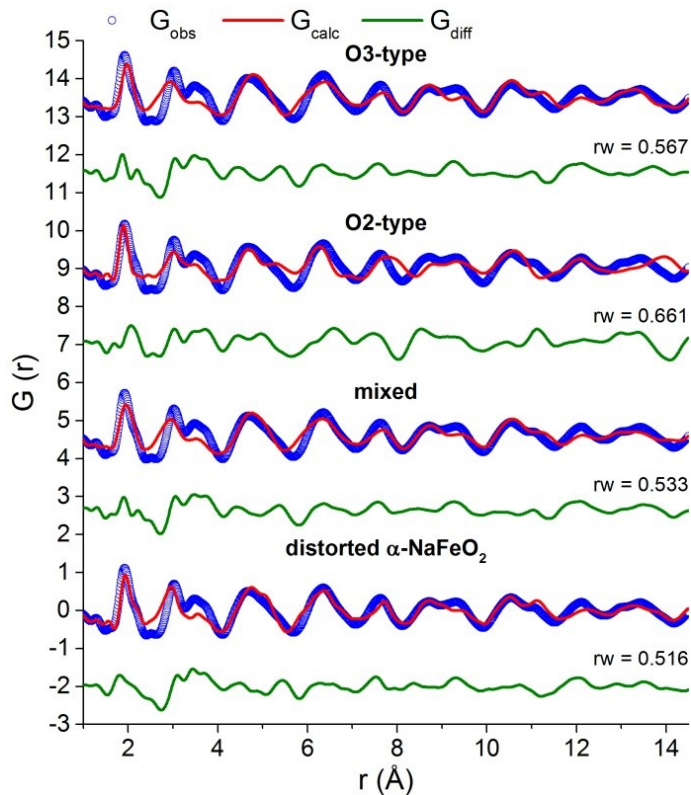


**Figure S8.** PDF fits to the chemically lithiated sample, from top and down O3-type, O2-type, mix and the distorted  $\alpha$ -NaFeO<sub>2</sub>. The O2-type was added as a second phase with scale factor  $s$ , while the scale factor of the O3-type was set to  $(1-s)$ , such that the chance of finding A after AB, i.e. the stacking fault probability, comes directly from  $s$ . This procedure has been described by Yang et. al.<sup>10</sup>

**Table S3.** overview of PDFfit results for the intermediate range ordering

	O3-type	O2-type	O3-type (aniso)	O2-type (aniso)	mix*	distorted (P2/m <sub>RUT</sub> )
rw	0.567	0.661	0.552	0.576	0.533	0.516
scale	0.150	0.124	0.155	0.195	0.161	0.164
$s$	-	-	-	-	0.218	-
$a$ (Å)	2.96	3.01	2.95	2.97	2.97	5.27
$b$ (Å)	-	-	-	-	-	2.91
$c$ (Å)	14.08	8.88	14.12	10.43	13.90	5.09
$\beta$ (°)	120	120	120	120	120	67.55
delta2	3.10	3.28	3.12	3.38	3.17	3.44
diameter (Å)	51.5	51.5	51.5	51.5	51.5	50.0
Ti U <sub>iso</sub>	0.0383	0.0222	-	-	0.0447	0.0461
U <sub>11</sub> , U <sub>22</sub>	-	-	0.0337	0.0268	-	-
U <sub>33</sub>	-	-	0.0694	0.1887	-	-
O U <sub>iso</sub>	0.0167	0.0217	-	-	0.0142	0.0057
U <sub>11</sub> , U <sub>22</sub>	-	-	0.0083	0.0105	-	-
U <sub>33</sub>	-	-	0.0444	0.0198	-	-

\* cell parameters relative to O3-type cell, locked such that  $c_{O2} = 2/3 c_{O3}$

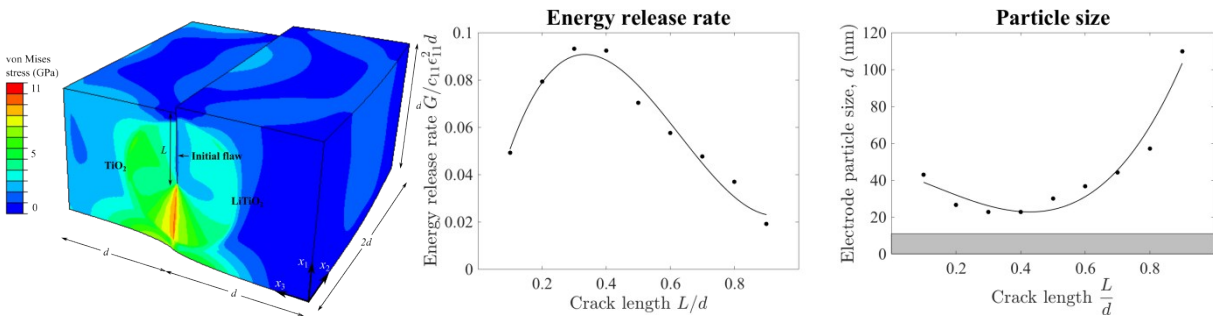


**Figure S9.** (a) The von Mises stress distribution on a deformed rutile electrode consisting of a crack-like flaw on the distorted lithiated rutile / distorted  $\alpha$ -NaFeO<sub>2</sub> ( $\text{Li}_{-0.75}\text{TiO}_2/\text{Li}_{-1}\text{TiO}_2$ ) phase boundary. (b) The energy release rate as a function of crack length in the rutile particle. (c) Particle size of rutile electrode below which fracture is suppressed as a function of initial flaw size. The shaded region corresponds to the typical rutile particles used in our experiments.

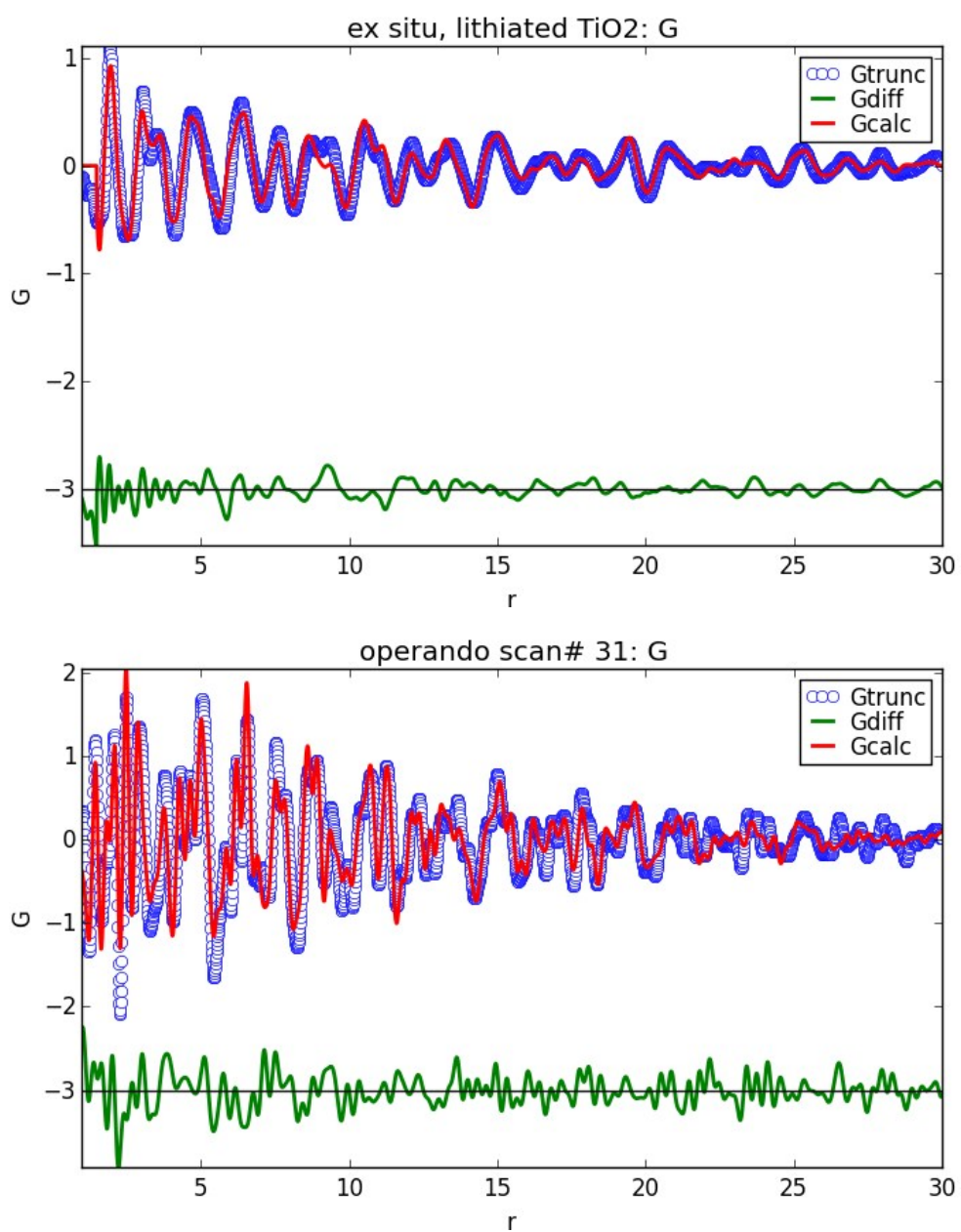


**Figure S10.** Comparison of the PDF fits for the ex situ and operando data for LiTiO<sub>2</sub>. The operando fit includes a local graphite structure as a second phase. The operando fit ( $R_w = 0.38$ ) is naturally not as good as for the ex situ data ( $R_w = 0.32$ ), as the signal intensity is decreased, and background noise caused by the AMPIX cell is increased as with fits of the pristine rutile TiO<sub>2</sub> material and the pristine electrode shown in Figure S1.

## References:

- (1) Kavan, L.; Grätzel, M.; Gilbert, S. E.; Klemenz, C.; Scheel, H. J. Electrochemical and Photoelectrochemical Investigation of Single-Crystal Anatase. *J. Am. Chem. Soc.* **1996**, *118* (28), 6716–6723.
- (2) Banfield, J. F.; Veblen, D. R. Conversion of Perovskite to Anatase and TiO<sub>2</sub> (B): A TEM Study and the Use of Fundamental Building Blocks for Understanding Relationships among the TiO<sub>2</sub> Minerals. *Am. Mineral.* **1992**, *77* (5–6), 545–557.
- (3) Cromer, D. T.; Herrington, K. The Structures of Anatase and Rutile. *J. Am. Chem. Soc.* **1955**, *77* (18), 4708–4709.
- (4) Baur, W. H. Über Die Verfeinerung Der Kristallstrukturbestimmung Einiger Vertreter Des Rutiltyps. II. Die Difluoride von Mn, Fe, Co, Ni Und Zn. *Acta Crystallogr.* **1958**, *11* (7), 488–490.
- (5) Marchand, R.; Brohan, L.; Tournoux, M. TiO<sub>2</sub>(B) a New Form of Titanium Dioxide and the Potassium Octatitanate K<sub>2</sub>Ti<sub>8</sub>O<sub>17</sub>. *Mater. Res. Bull.* **1980**, *15* (8), 1129–1133.
- (6) Latroche, M.; Brohan, L.; Marchand, R.; Tournoux, M. New Hollandite Oxides: TiO<sub>2</sub>(H) and K<sub>0.06</sub>TiO<sub>2</sub>. *J. Solid State Chem.* **1989**, *81* (1), 78–82.
- (7) Akimoto, J.; Gotoh, Y.; Oosawa, Y.; Nonose, N.; Kumagai, T.; Aoki, K.; Takei, H. Topotactic Oxidation of Ramsdellite-Type Li<sub>0.5</sub>TiO<sub>2</sub>, a New Polymorph of Titanium Dioxide: TiO<sub>2</sub>(R). *Journal of Solid State Chemistry*. 1994, pp 27–36.
- (8) Simons, P. Y.; Dachille, F. The Structure of TiO<sub>2</sub> II, a High-Pressure Phase of TiO<sub>2</sub>. *Acta Crystallogr.* **1967**, *23* (2), 334–336.
- (9) SATO, H.; ENDO, S.; SUGIYAMA, M.; KIKEGAWA, T.; SHIMOMURA, O.; KUSABA, K. Baddeleyite-Type High-Pressure Phase of TiO<sub>2</sub>. *Science (80-.)*. **1991**, *251* (4995), 786–788.
- (10) Yang, X.; Masadeh, A. S.; McBride, J. R.; Božin, E. S.; Rosenthal, S. J.; Billinge, S. J. L. Confirmation of Disordered Structure of Ultrasmall CdSe Nanoparticles from X-Ray Atomic Pair Distribution Function Analysis. *Phys. Chem. Chem. Phys.* **2013**, *15* (22), 8480.